Physica E 148 (2023) 115653

Contents lists available at ScienceDirect

Physica E: Low-dimensional Systems and Nanostructures

journal homepage: www.elsevier.com/locate/physe

Structural properties of femtosecond laser irradiation induced bismuth oxide based nano-objects in $Bi_{12}SiO_{20}$ (BSO) single crystal

Nebojsa Romcevic, Marina Lekic, Aleksander Kovacevic, Novica Paunovic, Borislav Vasic, Maja Romcevic *

Institute of Physics Belgrade, University of Belgrade, 11080, Belgrade, Serbia

ARTICLE INFO

Handling Editor: M.W. Wu

Keywords:
Czochralski technique
Laser modification
Nanocomposites
Far-infrared spectroscopy

ABSTRACT

Single crystal of $Bi_{12}SiO_{20}$ was grown from the melt by Czochralski technique. The crystal growth was in the [111] direction. The surface of the polished sample was irradiated by a femtosecond pulsed laser beam of various power. The influence of laser power on structural properties of $Bi_{12}SiO_{20}$ crystal, as well as on its phase composition, was studied. The surface morphology of our samples was investigated by AFM. The surface of unirradiated sample is rather smooth with no cracks observed. In sample modified by pulsed femtosecond beam, we registered the presence of small spherical islands on the surface. The dimensions of the islands and their density depend on the applied power. There were also significant changes in far-infrared spectra of irradiated sample in comparation to non-irradiated sample. Based on these results, the material obtained after femtosecond pulsed laser irradiation consisting of bismuth oxide based nano-objects, formed as nanocrystals (dimensions below 20 nm in diameter), which are arranged in a matrix of $Bi_{12}SiO_{20}$.

1. Introduction

Sillenites ($Bi_{12}MO_{20}$, M = Si, Ge, Ti) are optically active crystals exhibiting a lot of strong effects (optical rotation, electro-optical (Pockels), magneto-optical (Faraday) and photo-induced effects) and interesting properties such us remarkably large values of dielectric, piezo-electric and elasto-optic constants, very high values of the dark electric resistance, the index of refraction [1] etc. These crystals have application as active elements in many devices [2]. For these applications the materials are bulk single crystal samples.

On the other hand, due to their extremely small sizes, nanomaterials (one, two or three dimensions of less than 100 nm) cannot be used in large scale, particularly as long-bearing materials in engineering applications. For this it has long been a desire to develop bulk composites incorporating these nanomaterials (for example nanocomposites) to harness their extraordinary properties in bulk applicable materials. Initial ideas and principles are given in Ref. [3]. The most important fact is that the characteristics of the nanomaterials are fundamentally different in comparison with the bulk materials [4].

Lasers play an ever expanding role in material processing [5], as is the case with surface treatment of single crystals [6] where the energy of a laser beam interacts with a material to transform it in some way in a thin surface layer. This transformation (or laser process) is controlled by precisely regulating the wavelength, power, duty cycle and repetition rate of the laser beam. All materials have unique characteristics that dictate how the laser beam interacts and consequently modifies the material [7,8].

In our previous papers, we have investigated the influence of locally induced heating with increasing laser power densities on some nanomaterials such as stable hexagonal transition oxides ZnO doped with CoO [9] and cubic rock-salt MnO [10]. The influence of femtosecond pulsed laser power on the quality and optical characteristics of $Bi_{12}GeO_{20}$ single crystal was also studied [11].

The aim of this work is to continue our research with investigation influence of femtosecond pulsed laser irradiation on $Bi_{12}SiO_{20}$ single crystal using FTIR spectroscopy along with atomic force microscopy (AFM), but this time the focus is on modification of material and its structural characterization.

2. Experimental procedure

2.1. Preparation of crystal samples

Czochralski technique was applied to grow $Bi_{12}SiO_{20}$ single crystal,

* Corresponding author.
E-mail address: romcevic@ipb.ac.rs (M. Romcevic).

https://doi.org/10.1016/j.physe.2023.115653
Received 17 November 2022; Received in revised form 26 December 2022; Accepted 5 January 2023
Available online 6 January 2023

where MSR 2 crystal puller controlled by a Eurotherm was used with temperature fluctuations of the experiment lower than 0.2 °C. Additional weighing set was used to monitor the crucible weight in order to keep a crystal diameter constant (absolute deviation was below 0.1 mm).

A platinum crucible was used to contain the melt, which was placed in an alumina vessel on a zircon – oxide wool. This system was constructed in order to stop the excessive radiation heat losses. Also, a cylindrical silica glass after heater was constructed around the system to reduce the thermal gradients in the crystal and in the melt. Crystal growth was occurred in an air atmosphere while iridium wires were used as initial crystal seeds. Later on, seed cuts from the produced $Bi_{12}SiO_{20}$ crystals were used for the growth of other crystals.

Bi_2O_3 and SiO_2 were used for synthesis of crystals. Starting materials were mixed in 6:1 stoichiometric ratio. Optimal pull rate was chosen in the range 5 – 6 mm/h. Equations of the melt hydrodynamics were used to calculate critical crystal diameter, $d_c = 10$ mm and critical rotation, $\omega_c = 20$ rpm. The crucible was not rotating during crystal growth. The crystal boule was cooled at ~50 °C/h down to a room temperature, after the crystal growth. Crystals grew in [111] direction, without core being observed. Finally, crystals were cut and polished.

2.2. Crystal irradiation and characterization

Crystal samples were exposed to a pulsed femtosecond laser beam (pulse width 90 fs, repetition rate 76 MHz) from Coherent Mira 900 F laser system pumped by a 532 nm continuous wave Coherent Verdi V-10 laser. The irradiating beam wavelength was monitored by an Ocean Optics HR2000CG UV-NIR spectrometer. The samples were irradiated along their longest axis, z, i.e., along the crystal growth direction. During irradiation, the crystal facet was partially exposed due to the oval shape of the beam profile. A graded filter was used to adjust the beam power on the sample from 50 to 800 mW (measured by Ophir Nova II powermeter with thermal and photometric heads), which corresponds to the fluence range of 75–1200 nJ/cm^2. Exposure time of each irradiation power was 3s, measured by a stopwatch of 0.2s of accuracy. The total irradiation time and energy were intentionally kept low to avoid significant contribution of an accumulative process caused by repopulation of the traps [12].

Far-infrared reflection spectra were recorded in the wave number range up to 650 cm^{-1} utilizing an A BOMEM DA - 8 FTIR spectrometer with a deuterated triglycine sulfate (DTGS) pyroelectric detector.

The surfaces of samples were examined in detail using Atomic Force Microscope (AFM), NTEGRA prima from NT-MDT. NSG01 probes with a typical resonant frequency of 150 kHz and 10 nm tip apex curvature radius were used.

The X-ray diffraction (XRD) data for $Bi_{12}SiO_{20}$ single crystals was measured using X-ray diffractometer (XRD) Rigaku Ultima IV, Japan, with filtered CuKα1 radiation ($\lambda = 0.154178$ nm). The X-ray diffraction data were collected over the 2θ range from 20° up to 80° with the step of 0.02° and scanning rate of 2°/min. The PDXL2 v2.0.3.0 software [13], with reference to the diffraction patterns available in the International Center for Diffraction Data (ICDD) [14] was used for the phase identification and data analysis.

3. Results and discussion

3.1. Femtosecond pulsed laser modification

In order to establish the behaviour of the sample material under the influence of femtosecond beam, three wavelengths from the common range of the Mira device (700–900 nm) have been chosen. The samples were exposed to femtosecond beam of 730, 800 and 830 nm, with input powers of 50–700, 50–800, and 50–550 mW, respectively. For each wavelength, the transmitted power vs input power has been monitored. The input power has been gradually increased and in this way the influence of possible strong modifications by higher power to the results of low power was diminished. Transmitted vs. input power dependency was established (Fig. 1).

Transmitted power dependence on the input power is in fact linear for each chosen wavelengths. The linear dependence shows uniform absorption during the input power change – there were no significant damages in the material of the samples caused by the beam during exposition. If present, strong or large-scale structural changes inside the material would change the absorption coefficient which would lead to the deviation of the Pout vs. Pin (Fig. 1) dependence from the linear one.

Because of that, in the further analysis in this paper, under treated sample we will consider the sample modified with a laser line of 730 nm and a power of 700 mW as a representative one. In Fig. 2, a sample treated with 730 nm and a power of 50 mW was analyzed for comparison.

3.2. AFM

Fig. 2 shows the results of AFM measurements of the $Bi_{12}SiO_{20}$ single crystal and the same sample after being irradiated by a femtosecond pulsed laser beam. The surface of unirradiated sample is rather smooth with no cracks observed, and only traces of mechanical polishing can be seen in Fig. 2a. Fig. 2b and c. Show the surface of the sample after irradiated by a femtosecond pulsed laser with 730 nm and power of 50 mW and 700 mW respectively. Full lines at Fig. 2 a-c present directions in which the structure dimensions were determined. Height prolife on the surface and in the shine dots is shown in Fig. 2 d. For the treated samples, the nanoobject clearly stands out in the selected direction. It could be said that the height of the nano-object for both samples is in the range of about 10–15 nm, and that the height of the nanoobject increases with the increase in the power of the femtosecond laser. On the other hand, the diameter of these nano-objects is about 20 nm (Figs. 2b) and 15 nm (Fig. 2c). In addition, we note that the density of nano-objects is significantly higher in Fig. 2c.

Average roughness (Ra) for the samples shown in Fig. 2 a, b, c is 1.25 nm, 1.57 nm and 1.6 nm, respectively. Although the value for Ra is relatively small, i.e. the surface of the samples is relatively smooth, we can conclude that as a result of the femtosecond laser treatment, as well as when increasing the laser power, the value for Ra also increases, which is expected.

3.3. XRD measurements

Phase analysis using XRD of single crystal BSO samples are presented

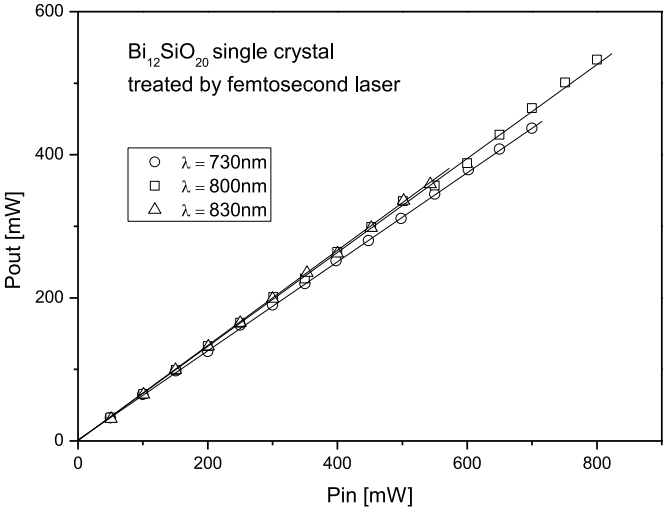

Fig. 1. Transmitted (Pout) vs. input (Pin) power for samples exposed to the beam of 730 nm, 800 nm and 830 nm.

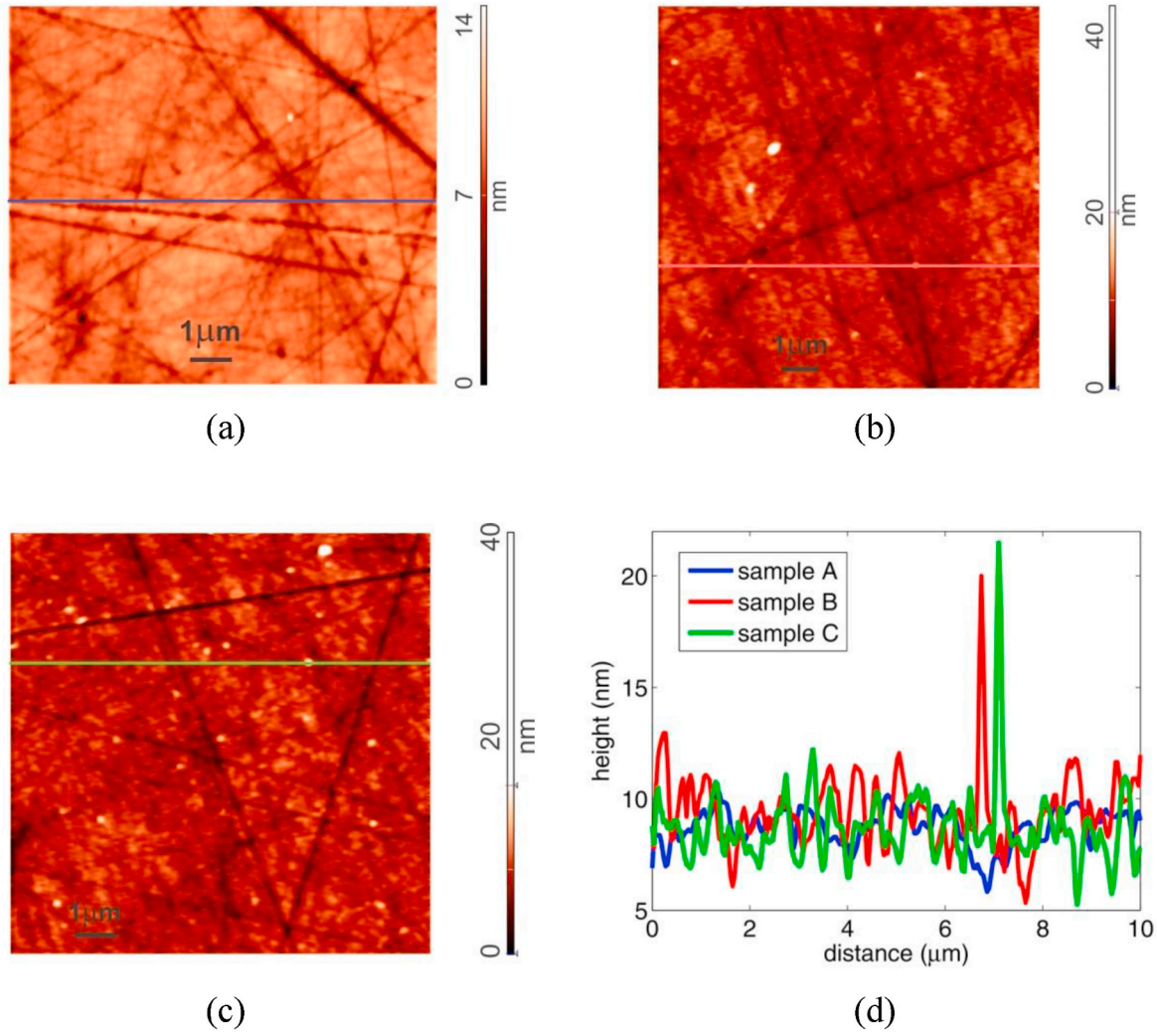

Fig. 2. AFM results of $Bi_{12}SiO_{20}$ single crystal: untreated (a); femtosecond laser treated sample: 730 nm, 50 mW (b) and 730 nm, 700 mW (c). Height prolife on the surface (d).

in Fig. 3. Phase analysis indicates that all peaks belong to the $Bi_{12}SiO_{20}$ phase, which is in good agreement with the JCPDF Card No. 37–0485.

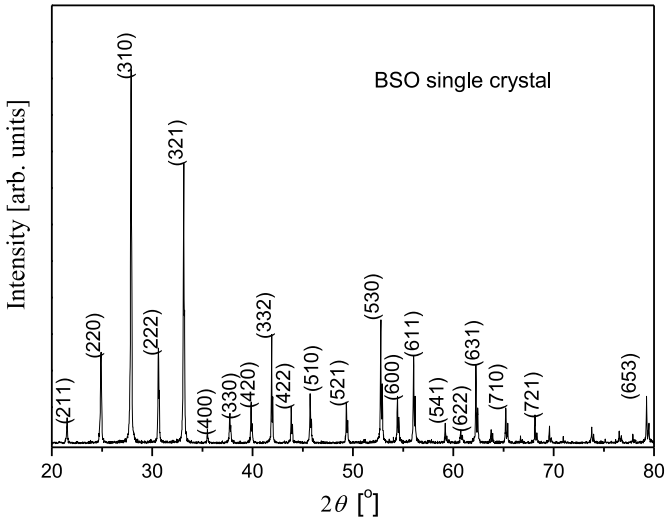

Fig. 3. X-ray diffraction results of untreated $Bi_{12}SiO_{20}$ single crystal, peaks of $Bi_{12}SiO_{20}$ phase marked with hkl.

The XRD for the treated sample is no different from that for the untreated.

3.4. Far-infrared spectroscopy

The experimental far-infrared spectrum of BSO single crystal was recorded in the spectral range of 70–650 cm^{-1} at room temperature and in Fig. 4 is presented as a blue line. The obtained spectrum shows all characteristics described in the literature [15,16]. The far-infrared spectrum of the femtosecond laser treated BSO, recorded in the spectral range of 70–650 cm^{-1} at room temperature, is presented in Fig. 4 as a red line. Even though the spectra given in Fig. 4 were recorded under the same conditions, differences in the BSO single crystal and femtosecond laser treated BSO spectra are clearly visible at in several places, such as about 130, 180, 280 cm^{-1} ….

$$\Gamma = 8A + 8E + 25F \quad (1)$$

Among these modes, only the F modes are infrared active.

Fig. 5, lower spectrum, shows the far-infrared spectra of BSO single crystal. The points are given the experimental results, and the solid line is obtained in the standard way by the procedure of fitting parameters [18,19]. Due to the large energy gap (Eg = 2,57eV) and accordingly very low concentrations of free carriers, a dielectric function was used which takes into account only the interaction of electromagnetic radiation with

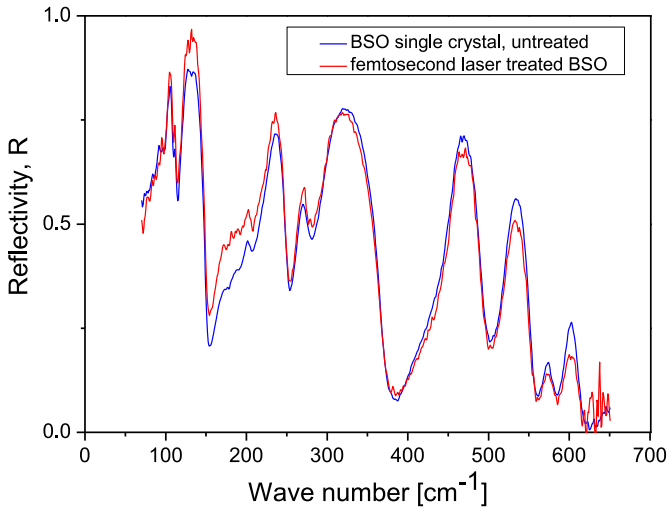

Fig. 4. Experimental far-infrared reflection spectra of $Bi_{12}SiO_{20}$ single crystal untreated (blue line) and treated by femtosecond beam (red line). First, in short about factor group analysis. Crystal BSO has a cubic unit with space group I23 (T3) [17].

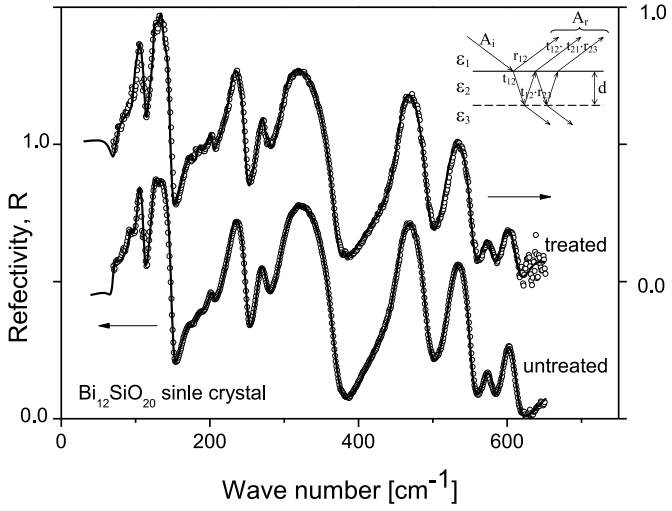

Fig. 5. Far-infrared reflection spectra of $Bi_{12}SiO_{20}$ single crystal and femtosecond laser-treated $Bi_{12}SiO_{20}$ sample. The experimentally obtained data points are depicted as circles. The theoretical spectrum obtained with the model defined by eqs. (2) and (3) and fitting procedure is given as solid line. Insert. Schematic overview of the femtosecond laser-treated $Bi_{12}SiO_{20}$ sample.

phonons:

$$\varepsilon(\omega) = \varepsilon_\infty \prod_{k=1}^{s} \frac{\omega^2 + i\gamma_{kLO} - \omega_{kLO}^2}{\omega^2 + i\gamma_{kTO} - \omega_{kTO}^2} \tag{2}$$

where ε_∞ is the bound charge contribution and is considered as a constant, ω_{LOk} and ω_{TOk} are the longitudinal and transverse optical – phonon frequencies, and γ_{TOk} and γ_{LOk} are the phonon dampings.

The results obtained for TO/LO frequencies (in cm^{-1}) are: 69/71, 94/95, 104/112, 123/150, 129.5/130, 142/143, 175.2/175.5, 187.5/192.5, 202.5/204.3, 229/251, 267/276.8, 297.5/371, 424/427, 453/494, 520/551.5, 572/581, 594/613, 647/658. The agreement with the literature data [15,16] is excellent. This result serves as an introduction to the spectrum analysis for the femtosecond laser treated BSO sample, where the situation is somewhat more complex. Fig. 5, upper spectrum, shows the far-infrared spectrum of femtosecond laser treated BSO single crystal. The points are given the experimental results, and the solid line is obtained in the following way.

Namely, as can be seen from Fig. 2b and c, laser treatment leads to a change in the surface of the samples. It seems that its composition changes in a very thin layer, but also that nanoobjects are formed inside the layer and on its surface. Therefore, we decided to use a model that takes into account the existence of a three-layer structure (see insert of Fig. 5), where.

(a) medium 1 is air ($\varepsilon_1 = 1$),
(b) medium 2 is a layer with thickness d present at the sample surface with dielectric constant ε_2 (eq. (2)), and
(c) lower optically thick layer, medium 3, practically single crystal BSO, described with ε_3 (eq. (2)).

In this case, the reflectivity can be determined as described in Ref. [20]:

$$R_A = \frac{A_r}{A_i} = \frac{\boldsymbol{r}_{12}e^{-i\alpha} + r_{23}e^{i\alpha}}{e^{-i\alpha} + \boldsymbol{r}_{12}\boldsymbol{r}_{23}e^{i\alpha}} \tag{3}$$

where $r_{ij} = (n_i - n_j)/(n_i + n_j) = (\sqrt{\varepsilon_i} - \sqrt{\varepsilon_j})/(\sqrt{\varepsilon_i} + \sqrt{\varepsilon_j})$ are the Fresnel coefficients, A_i and A_r represent amplitudes of the incident and reflection beams, respectively, n is the complex index of refraction, ε is the dielectric constant and $\alpha = 2\pi\omega d\ (\varepsilon_2)^{1/2}$ is the complex phase change related to the absorption in the crystal layer with the thickness d. Reflectance, R, is given as $R = |R_A|^2$.

The parameters of the treated sample were determined by the fitting procedure. In that manner, the parameters for the single crystal BSO layer (medium 3) remained the same as those determined from untreated sample. The surface layer (medium 2), besides them, has additional modes. The layer thickness is d = 1,9 μm. Comparison of our result with the values from the literature for the registered additional phonons is given in Table 1.

Some results from literature, for example [22], show that laser-induced oxidation of bismuth can occur, but the degree of oxidation and the formation of the crystalline phase strongly depend on the laser power. We think that in our case, due to laser heating, on the $Bi_{12}SiO_{20}$ single crystal, the formation of starting material phases occurs. It is known that bismuth oxide can exist in several polymorphic forms: α-Bi_2O_3, the only phase stable at room temperature, and three high-temperature phases, β-, δ- and γ-Bi_2O_3. The orthorhombic phase, α-Bi_2O_3, transforms to cubic δ-Bi_2O_3 at 729 °C, which may transform to tetragonal β-Bi_2O_3 or body-centered cubic γ-Bi_2O_3 upon cooling to 650 and 639 °C, respectively [24–27]. Both of these forms are metastable,

Table 1
Comparison between additional far-infrared frequencies registered in this paper and experimentally and calculated frequencies from the literature.

Phonon peaks This work [cm^{-1}]	Experimental literature values of phonon frequencies [cm^{-1}]	Calculated phonon frequencies [cm^{-1}]	Description
120	120 [21]	120 [21]	Bi_4O_7 [21]
	118 [22]		α-Bi_2O_3 [22]
		124 [21]	β-Bi_2O_3 [21]
161	157 [21]		γ-Bi_2O_3 [21]
	166 [23]		γ-Bi_2O_3 [23]
278	279 [22]		γ-Bi_2O_3 [22]
	281 [21]		γ-Bi_2O_3 [22]
380	381 [21]		γ-Bi_2O_3 [21]
		388 [21]	Bi_4O_7 [21]

but may be stabilized at room temperature by the addition of impurities [25].

Another metastable phase, which was also registered by our measurements, is Bi_4O_7. This phase is a fully chargeordered pseudo-binary bismuth (Bi^{3+}, Bi^{5+}) oxide [28,29]. This mixed valence and the optical gap within the visible range (1.9eV) turns the Bi_4O_7 interesting for applications in photocatalysis. Also, because of strong luminescence at about 420 nm Bi_4O_7 is a candidate as for purplish-blue light emitter [30]. One of the following directions of research can be dedicated to this topic as well.

It seems to us that in this way it is clearly shown that femtosecond laser treating produces nano-objects consisting of different phases based on bismuth oxide in a matrix of $Bi_{12}SiO_{20}$ single crystal. In the future, we will search for new functionalities, which would open up new topics and areas.

4. Conclusions

We used a femtosecond pulsed laser to modify the surface on a $Bi_{12}SiO_{20}$ single crystal growth by Czochralski technique. The treatment led to the formation of bismuth oxide based nanoobjects in the $Bi_{12}SiO_{20}$ matrix. These nanoobjects are formed as nanocrystals with dimensions below 20 nm in diameter and about 15 nm in height. By composition, they are α-, β-, and γ-Bi_2O_3 and Bi_4O_7. The concentration of nanoobjects increases when the power of the femtosecond laser increases. Application in optoelectronics and optical sensor industry is expected.

Author contributions

N. Romcevic: Conceptualization, Methodology, Formal analysis, Writing- Original draft preparation. **N. Paunovic, M. Lekic, A. Kovacevic, B. Vasic:** Investigation, Formal analysis. **M. Romcevic:** Investigation, Formal analysis, Writing—review and editing. All authors have read and agreed to the published version of the manuscript.

Funding

This research was supported by the Science Fund of the Republic of Serbia, Grant No. 7504386, Nano object in own matrix – Self composite – NOOM-SeC.

Declaration of competing interest

The authors declare that they have no known competing financial interests or personal relationships that could have appeared to influence the work reported in this paper

Data availability

Data will be made available on request.

References

[1] J.-C. Chen, L.-T. Liu, C.-C. Young, A study of the growth mechanism of bismuth silicon oxide during LHPG method, J. Cryst. Growth 198/199 (1999) 476–481, https://doi.org/10.1016/S0022-0248(98)01142-7.
[2] M.P. Petrov, A.V. Khomenko, in: P. Gunter, J.P. Huignard (Eds.), Photorefractive Materials and Their Applications II, Publicher, Springer, Berlin, 1989, pp. 325–352, https://doi.org/10.1007/BFb0120157.
[3] Y. Dzenis, Structural nanocomposites, Science 319 (2008) 419–420, https://doi.org/10.1126/science.1151434.
[4] T.E. Twardowski, Introduction to Nanocomposites Material Properties, Processing, Characterization, Publicher: Destech Publications, Lancaster, Pa, USA, 2007, pp. 1–532.
[5] P.M. Ossi, M. Dinescu, Laser processing of materials, in: P. Schaaf (Ed.), Springer Series in Materials Science (SSMATERIALS), vol. 139, 2010, pp. 131–167, https://doi.org/10.1007/978-3-642-13281-0.
[6] M.A. Montealegre, G. Castro, P. Rey, J.L. Arias, P. Vazquez, M. Gonzalez, Surface treatments by laser technology, Contemporary Materials I−1 (2010) 19–30, https://doi.org/10.5767/anurs.cmat.100101.en.019M.
[7] A.K. Roy (Ed.), Hybrid Atomic-Scale Interface Design for Materials Functionality, Publicher, Elsevier, 2021, https://doi.org/10.1016/C2018-0-05143-9.
[8] M.V. Shugaev, C. Wu, O. Armbruster, A. Naghilou, N. Brouwer, D.S. Ivanov, T.J.-Y. Derrien, N.M. Bulgakova, W. Kautek, B. Rethfeld, L.V. Zhigilei, Fundamentals of ultrafast laser–material interaction, MRS Bull. 41 (12) (2016) 960–968, https://doi.org/10.1557/mrs.2016.274.
[9] B. Hadzic, N. Romcevic, D. Sibera, U. Narkiewicz, I. Kurylisyn-Kudelska, W. Dobrowolski, M. Romcevic, Laser power influence on Raman spectra of ZnO (Co) nanoparticles, J. Phys. Chem. Solid. 91 (2016) 80–85, https://doi.org/10.1016/j.jpcs.2015.12.008.
[10] B. Hadzic, B. Vasic, B. Matovic, I. Kuryliszyn-Kudelska, W. Dobrowolski, M. Romcevic, N. Romcevic, Influence of laser induced heating on MnO nanoparticles, J. Raman Spectrosc. 49 (5) (2018) 817–821, https://doi.org/10.1002/jrs.5358.
[11] A. Kovacevic, J. Ristic-Djurovic, M. Lekic, B. Hadzic, G. Saleh Isa Abudagel, S. Petricevic, P. Mihailovic, B. Matovic, D. Dramlic, Lj Brajovic, N. Romcevic, Influence of femtosecond pulsed laser irradiation on bismuth germanium oxide single crystal properties, MRS Bull. 83 (2016) 284–289, https://doi.org/10.1016/j.materresbull.2016.06.023.
[12] B. Taheri, S.A. Holmstrom, R.C. Powell, J.J.F. Song, F. Antonio Munoz, I. Földvári, A. Péter, Nonlinear absorption of laser light in $Bi_{12}GeO_{20}$ single crystals, Opt. Mater. 3 (1994) 251–255, https://doi.org/10.1016/0925-3467(94)90037-X.
[13] PDXL Version 2.0.3.0 Integrated X-Ray Powder Diffraction Software, Rigaku Corporation, Tokyo, Japan, 2011, p. 196.
[14] Powder Diffraction File, PDF-2 Database, Announcement of New Database Release, International Centre for Diffraction Data (ICDD), 2012.
[15] A. Golubovic, S. Nikolic, R. Gajic, S. Duric, A. Valcic, The grown and optical properties of $Bi_{12}SiO_{20}$ single crystals, J. Serb. Chem. Soc. 67 (4) (2002) 279–289.
[16] D. Senuliene, G. Babonas, Far infrared reflection spectra of sillenite crystals and their solid solutions, phys. stat. solidi (b) 180 (2) (1993) 541–549, https://doi.org/10.1002/pssb.2221800225.
[17] G.N. Zhizhin, B.N. Mavrin, V.F. Shabanov, Opticheskie Kolebatelnye Spektry Kristallov, Pubisher: Nauka, Moskva, 1984.
[18] J. Trajic, M. Romcevic, N. Romcevic, B. Babic, B. Matovic, P. Balaz, Far-infrared spectra of mesoporous ZnS nanoparticles, Opt. Mater. 57 (2016) 225–230, https://doi.org/10.1016/j.optmat.2016.05.004.
[19] J. Trajic, M. Rabasovic, S. Savić-Sevic, D. Sevic, B. Babic, M. Romcevic, J. Ristic-Durovic, N. Paunovic, J. Krizan, N. Romcevic, Far-infrared spectra of dysprosium doped yttrium aluminium garnet nanopowder, Infrared Phys. Technol. 77 (2016) 226–229, https://doi.org/10.1016/j.infrared.2016.06.003.
[20] M. Gilic, J. Trajic, N. Romcevic, M. Romcevic, D.V. Timotijevic, G. Stanisic, I. S. Yahia, Optical properties of CdS thin films, Opt. Mater. 35 (2013) 1112–1117, https://doi.org/10.1016/j.optmat.2012.12.028.
[21] O. Depablos-Rivera, A. Martinez, S.E. Rodil, Interpretation of the Raman spectra of bismuth oxide thin films presenting different crystallographic phases, J. Alloys Compd. 853 (2021), 157245, https://doi.org/10.1016/j.jallcom.2020.157245.
[22] K. Trentelman, A note on the characterization of bismuth black by Raman microspectroscopy, J. Raman Spectrosc. 40 (2009) 585–589, https://doi.org/10.1002/jrs.2184.
[23] C. Rodriguez-Fernandez, K. Akius, M.M. de Lima Jr., A. Cantarero, J.M. van Ruitenbeek, C. Sabater, Raman signal revels the rhombohedral crystallographic structure in ultra-thin layers of bismut thermally evaporated on amprphous substrate, Maerials Sci. Eng. B 27 (2021), 115240, https://doi.org/10.1016/j.mseb.2021.115240.
[24] S. Venugopalan, A.K. Ramdas, Raman spectra of bismuth germanium oxide and bismut silicon oxide, Phys. Rev. B 8 (10) (1972) 4065–4079, https://doi.org/10.1103/PhysRevB.5.4065.
[25] B. Mihailova, M. Gospodinov, L. Konstantinov, Raman spectroscopy study of silenites. I. Comparasion between $Bi_{12}(Si,Mn)O_{20}$ single crystals, J. Phys. Chem. Solid. 60 (1999) 1821–1827, https://doi.org/10.1016/S0022-3697(99)00194-8.
[26] I.F. Vasconcelos, M.A. Pimenta, A.S.B. Sombra, Optical properties of $Bi_{12}SiO_{20}$ (BSO) and $Bi_{12}TiO_{20}$ (BTO) obtained by mechanical alloying, J. Mater. Sci. 36 (2001) 587–592, https://doi.org/10.1023/A:1004804000723.
[27] J.C. Alonso, R. Diamant, E. Haro-Poniatowski, M. Fernandez-Guasti, G. Munoz, I. Camarillo, M. Jouanne, J.F. Morhange, Raman characterization of $Bi_{12}SiO_{20}$ thin films obtained by pulsed laser deposition, App. Sur. Sci. 109/110 (1997) 359–361, https://doi.org/10.1016/S0169-4332(96)00674-5.
[28] B. Begemann, M. Jansen, Bi_4O_7, das erste definierte binare Bismut (III, V) - oxid, J. Less Common. Met. 156 (1989) 123–135, https://doi.org/10.1016/0022-5088(89)90412-8.
[29] R.E. Dinnebier, R.M. Ibberson, H. Ehrenberg, M. Jansen, The crystal structures of the binary mixed valence compound $Bi(III)_3Bi(V)O_7$ and isotypic Bi_3SbO_7 as determined by high resolution X-ray and neutron powder diffraction, J. Solid State Chem. 163 (2002) 332–339, https://doi.org/10.1006/jssc.2001.9427.
[30] H. Guan, Y. Feng, Facile synthesis and purplish blue luminescence of the binary mixed valence compound Bi_4O_7 microcrystals, Matter. Lett. 143 (2015) 269–272, https://doi.org/10.1016/j.matlet.2014.12.129.